Promoting the ambient-condition stability of Zr-doped barium cerate: Toward robust solid oxide fuel cells and hydrogen separation in syngas

Yang, Y.; Zeng, Y.; Amirkhiz, B.S.; Luo, J.-L.; Yan, N.

DOI
10.1016/j.jpowsour.2017.12.036

Publication date
2018

Document Version
Final published version

Published in
Journal of Power Sources

Journal of Power Sources 378 (2018) 134–138

Contents lists available at ScienceDirect

Journal of Power Sources

journal homepage: www.elsevier.com/locate/jpowsour

Promoting the ambient-condition stability of Zr-doped barium cerate: Toward robust solid oxide fuel cells and hydrogen separation in syngas

Ying Yang[b], Yimin Zeng[d], Babak S. Amirkhiz[d], Jing-Li Luo[c], Ning Yan[a,*]

[a] Van't Hoff Institute for Molecular Sciences (HIMS), University of Amsterdam, Amsterdam, 1098XH, The Netherlands
[b] Department of Mechanics and Engineering Structure, Wuhan University of Technology, No.22 Luoshi Road, 430070, Wuhan, Hubei, China
[c] Department of Chemical and Materials Engineering, University of Alberta, Edmonton, Alberta, T6G 1H9, Canada
[d] CanmetMATERIALS, Natural Resources Canada, Hamilton, Ontario, L8P 0A5, Canada

HIGHLIGHTS

- Various Zr-doped barium cerates can suffer surface degradation in ambient air.
- 10 mol% doping of Sn improves ambient-condition stability of cerates.
- Sn-doped cerate shows good performances in SOFC and H_2 permeation tests.

ARTICLE INFO

Keywords:
Perovskite oxide
Proton-conducting membrane
Chemical stability
Solid oxide fuel cells
Hydrogen permeation

ABSTRACT

Increasing the stability of perovskite proton conductor against atmospheric CO_2 and moisture attack at ambient conditions might be equally important as that at the elevated service temperatures. It can ease the transportation and storage of materials, potentially reducing the maintenance cost of the integral devices. In this work, we initially examined the surface degradation behaviors of various Zr-doped barium cerates ($BaCe_{0.7}Zr_{0.1}Y_{0.1}Me_{0.1}O_3$) using XRD, SEM, STEM and electron energy loss spectroscopy. Though that the typical lanthanide (Y, Yb and Gd) and In incorporated Zr-doped cerates well resisted CO_2-induced carbonation in air at elevated temperatures, they were unfortunately vulnerable at ambient conditions, suffering slow decompositions at the surface. Conversely, Sn doped samples (BCZYSn) were robust at both conditions yet showed high protonic conductivity. Thanks to that, the anode supported solid oxide fuel cells equipped with BCZYSn electrolyte delivered a maximum power density of 387 mW cm^{-2} at 600 °C in simulated coal-derived syngas. In the hydrogen permeation test using BCZYSn based membrane, the H_2 flux reached 0.11 mL cm^{-2} min^{-1} at 850 °C when syngas was the feedstock. Both devices demonstrated excellent stability in the presence of CO_2 in the syngas.

1. Introduction

Perovskite structured oxides have garnered tremendous attention over the past decades as a promising series of high-temperature proton conductors [1–4]. They constitute the electrolyte of proton-conducting solid oxide fuel cells (PC-SOFCs) that are advantageous, in terms of the efficiency, over the conventional ones based on the oxygen ionic conductor [5]. Thanks to the excellent protonic conductivity, PC-SOFCs work nicely at a much lower temperature. This significantly reduces the materials cost and boosts the long-term stability [6–8]. Recent work has demonstrated that PC-SOFCs maintained superior performances at temperature as low as 350 °C after hundreds of hours of operation [8]. In addition, the reactors derived from PC-SOFCs also show the capabilities for alternative applications including alkene dehydrogenation, water electrolysis and CO_2 conversions [9–11]. The hydrogen pump is another key application of the perovskite proton conductor. After compositing with a suitable electronic conductor, this hybrid membrane enables spontaneous hydrogen separation with excellent selectivity [4,12]. Because no external power supply is required, this approach offers outstanding energy efficiency compared to the conventional pressure swing adsorption and the cryogenic separation techniques [13].

A wide variety of perovskite oxides exhibit protonic conductivity at elevated temperatures [1,2]. This includes doped $BaCeO_3$, $BaZrO_3$, $SrCeO_3$, $SrZrO_3$ and $LaNbO_3$, among which Y-doped barium cerates prevail owing to their excellent ionic conductivity and sinterability. Co-doping cerates using a secondary trivalent cation, e.g., Yb and Gd [14,15], can further optimize the transport properties. Nonetheless,

* Corresponding author.
E-mail address: n.yan@uva.nl (N. Yan).

https://doi.org/10.1016/j.jpowsour.2017.12.036
Received 8 October 2017; Received in revised form 12 December 2017; Accepted 13 December 2017
Available online 22 December 2017

many cerates are instable at elevated temperature when exposing to acidic gases (e.g., CO_2 and H_2O) [16]. Their detrimental reactions cause the decomposition of cerates and often degrade the performances of the devices. Conversely, barium zirconate is much robust, well resisting the CO_2 attack at high temperatures [16,17]. But its conductivity is much lower than that of cerate. To enhance the chemical stability and maintain the high protonic conductivity of cerate, incorporating Zr is logically and practically the most viable solution. In particular, 10–30 mol.% Zr doped cerates are of great research interest [11,12,15,18–20]. Because of their good proton conductivity and reasonable stability in mild environment at high temperatures, they have been widely applied as the membrane materials for PC-SOFC and hydrogen pump.

Despite their excellent high temperature properties, we recently discovered that the 10 mol.% zirconium doped barium cerate suffered slow degradation at ambient conditions [21], posing a great challenge for the transportation and storage of the material and potentially increasing the maintenance cost of the integral devices. In this work, we initially investigated the ambient-condition stability of $BaCe_{0.7}Zr_{0.1}Y_{0.1}Yb_{0.1}O_3$, one of the classical perovskite proton conducting materials [15], and screened a number of acceptor and isovalent dopants in order to promote the robustness of cerates. The Sn doped cerate demonstrated excellent stability at both ambient and working conditions, enabling excellent yet robust PC-SOFC and hydrogen separation performances in simulated coal-derived synthesis gas.

2. Experimental

2.1. Materials preparations

The conventional sol-gel method was used to prepare the perovskite oxide powders with varied compositions, including $BaCe_{0.7}Zr_{0.1}Y_{0.2}O_3$ (BCZY), $BaCe_{0.7}Zr_{0.1}Y_{0.1}Yb_{0.1}$ (BCZYYb), $BaCe_{0.7}Zr_{0.1}Y_{0.1}Sn_{0.1}$ (BCZYSn), $BaCe_{0.7}Zr_{0.1}Y_{0.1}In_{0.1}$ (BCZYIn) and $BaCe_{0.7}Zr_{0.1}Y_{0.1}Gd_{0.1}$ (BCZYGd). Initially, stoichiometric amounts of metal (oxy)nitrates were dissolved into deionized water with vigorous stirring. Then appropriate amounts of ethylenediaminetetraacetic acid (EDTA, from Acros-organis) and citric acid (CA, from Sigma-Aldrich) were added as the chelating agents. The molar ration of total metal ions: EDTA: CA was 1.5: 1: 1. The subsequent mild heating under constant agitation induced water evaporation and the gelation of the residual. The obtained gel was finally calcined at 1200 °C for 10 h to form the desired phases. Similarly, $Gd_{0.1}Ce_{0.9}O_2$ (GDC) and $PrBaCo_2O_{5+\delta}$ (PBC) powders were prepared using the same method. Glycine, however, was used as the chelating agent instead of EDTA and CA.

2.2. Materials characterizations

The powder X-ray diffraction (XRD) was performed on a Rigaku Miniflex X-ray diffractometer using CuK_α radiation (λ = 1.54056 Å). The 2-theta range was 10-90° with the step size of 0.02° and the scan rate of 2.5° min^{-1}. The morphology of the sample was characterized using a FEI Verios 460 scanning electron microscope (SEM) coupled with an energy-dispersive X-ray (EDX) detector. Transmission electron microscope (TEM) analysis was carried out using a FEI Tecnai Osiris TEM operating at 200 kV. It was equipped with a high angle annular dark field (HAADF) scanning transmission electron microscope (STEM) detector coupled with an EDX spectrometer for elemental analysis. The sample was prepared by spreading a small amount of the powder, dispersed in ethanol, onto the copper grid. Thermogravimetric and differential scanning calorimetric (TGA-DSC) analysis was carried out using the NETZSCH Jupiter® STA 449F3. All the measurements were done in the temperature range of 30–900 °C in air flow with a flow rate of 20 mL min^{-1} at a heating rate of 5 °C min^{-1}.

2.3. Procedures of cerate stability test

The ambient-condition stability test of various cerates was carried out at room temperature (21 °C) in humidified ambient air (relative humidity = 98–100%). The sample powder was placed and sealed in a quartz tube. Humidified air was continuously passed through for 72 h. The stability test of BCZYSn in simulated coal-derived syngas (40% H_2 + 60% CO, certified and provided by Praxair, Inc.) was performed likewise. The tube was mounted in a tubular furnace to be heated to the designed temperatures.

2.4. Procedures of electrochemical test

A detailed PC-SOFC button cells fabrication procedure was reported in our previous work [22]. In brief, the BCZYSn electrolyte ink was spin-coated on the pre-calcined porous NiO-BCZYSn support, a subsequent 5 h sintering at 1420 °C fully densified the electrolyte. Then the PBC-BCZYSn cathode ink was applied onto the opposite side of the dense electrolyte to form the cathode after 2 h calcination at 1000 °C. In the electrochemical test, gold paste was applied onto both electrodes as the current collector. The button cell was mounted between a pair of coaxial alumina tube in the furnace. Before the test, the cell was reduced in a stream of 5% H_2 + N_2 and then conditioned in humidified H_2 (*ca.* 3 vol % water vapor). During the test, the impedance and current–voltage characteristics were determined using a Solartron 1287 electrochemical interface together with a 1255B frequency response analyzer. The hydrogen flow rate was 50 mL min^{-1} whereas the oxygen flow rate at the cathode was also 50 mL min^{-1}. The conductivity of the BCZYSn disc was determined at the designed temperatures in humidified hydrogen environment using the two-electrode configuration via the electrochemical impedance spectroscopy. All the impedance spectra were obtained under open circuit with the AC amplitude of 10 mV and the frequency range from 0.1 Hz to 100 kHz.

2.5. Procedures of hydrogen permeation test

To prepare the hydrogen permeation membrane, equal amount of BCZYSn and GDC powders were homogenized thoroughly by ball milling in isopropanol. The dried mixture was pressed into pellet and densified at 1400 °C for 10 h. The obtained membrane disc was grinded and polished at both sides; the final thickness was controlled at 0.6–0.7 mm. The SOFC test setup was adapted and used to measure the hydrogen permeability. Before mounting to this setup, Pt paste was applied onto both sides of the disc as the porous catalytic layer for hydrogen activation. In the test, hydrogen was separated from both 50% H_2 balanced by He and the simulated coal-derived syngas; Ar was used as the sweep gas at the permeate side. The flow rates were 100 mL min^{-1} at both the feed and permeate sides. All the gas composition analysis was determined by the gas chromatography (GC, Agilent 6890N).

3. Results and discussion

3.1. Surface degradation of doped cerate at ambient conditions

Thermodynamically, pure $BaCeO_3$ and $BaZrO_3$ are both instable below 500 °C (see Fig. 1a). For instance, the ΔG reaches -95 kJ mol^{-1} at 25 °C for the carbonation reaction of $BaZrO_3$. Fortunately, the sluggish kinetics of such degradation at ambient conditions often suppresses the progress of the reaction. However, with the presence of high-level humid, this detrimental reaction might proceed rapidly. To examine the kinetically stability at ambient condition, we selected BCZYYb, one of the classical proton-conducting materials that exhibits high proton conductivity and reasonable chemical stability at high temperatures, as the studying sample. The STEM-HAADF image in Fig. 1b shows the morphologies of BCZYYb powder after the 72 h stability test in humid

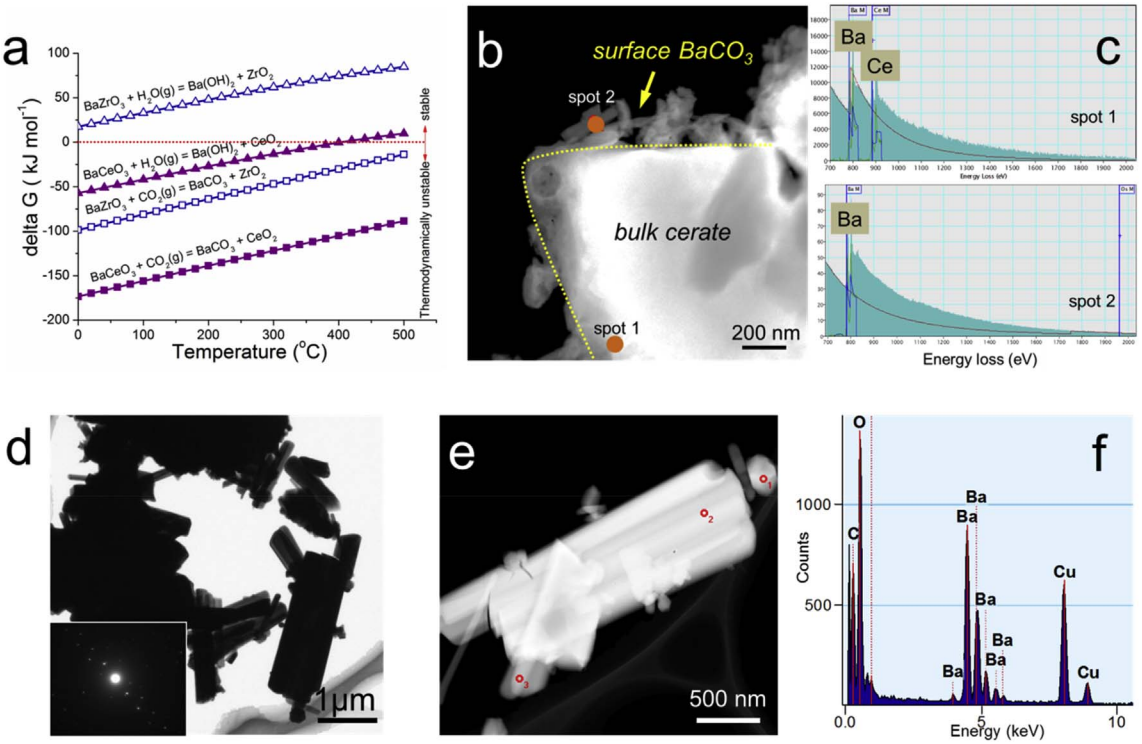

Fig. 1. (a) Thermodynamic calculations of barium cerate and zirconate decomposition reactions; (b) STEM-HAADF image of degraded BCZYYb; (c) the EELS spectra at spots 1 and 2 in (b); (d) bright field TEM micrograph of surface nanorods and the electron diffractogram (inset); (e) STEM-HAADF image of a nanorod and the (f) corresponding EDX spectrum.

air. Similar to our previous observations [21], the characteristic nanorods were found at the surface of BCZYYb. Both the EELS and EDX elemental analyses indicated that these nanorods contained exclusively barium without other metallic elements. The electron diffractogram in Fig. 1d and the XRD analysis (see below) further verified that the Ba-rich phases were indeed $BaCO_3$. However, this surface degradation was not observed when treating the sample with either dry air or dry CO_2, implying that such decomposition must be also "catalyzed" by moistures [21].

3.2. Improving the ambient-condition stability

To further examine the ambient-condition stability of cerates, a number of acceptor and isovalent dopants have been incorporated into its lattice. Representatives from lanthanide (Gd, Y, Yb), group 13 (In) and group 14 (Sn) elements were selected, which have been reported to be capable of boosting the proton conductivity and/or chemical stability of cerates. The doping ratios were all kept at 10 mol.% at the B site of the perovskite. Fig. 2a shows the XRD patterns of the as-prepared BCZYYb, BCZY, BCZYSn, BCZYIn and BCZYGd powder samples, confirming the successful formation of perovskite structure with few impurities. These samples were then subjected to the stability test for 72 h (*vide supra*). The crystallographic data in Fig. 2b indicates the partial structural destruction of BCZY, BCZYYb and BCZYGd. Two additional peaks, corresponding to the formation of $BaCO_3$, presented at *ca.* 25° and 35°, respectively. This suggested that the decomposition might follow the pathway below:

$$BaCe_{0.7}Zr_{0.1}Me_{0.2}O_3 + CO_2 + H_2O \rightarrow BaCO_3 + CeO_2 + MeC_xH_yO_z + ZrO_2 \quad (1)$$

Me is the lanthanide metals whereas $MeC_xH_yO_z$ represents the possible mixture of oxide, (oxy)hydroxide and (oxy/bi)carbonate. The diffraction patterns CeO_2 and ZrO_2 were, however, negligible because of their low quantity and the amorphous nature [21].

Conversely, no impurity has been identified by the XRD in the In and Sn doped samples, implying their enhanced ambient-condition stability. These air-treated samples were also analyzed by the TGA technique in Fig. 2c. Clearly, no significant weight loss was recorded for BCZYSn, the trivial mass variation might come from the change of the non-stoichiometric oxygen. The weight loss of BCZY, BCZYGd and BCZYYb increased progressively, suggesting the increased vulnerability. This trend was in good agreement with the intensity of $BaCO_3$ peak in

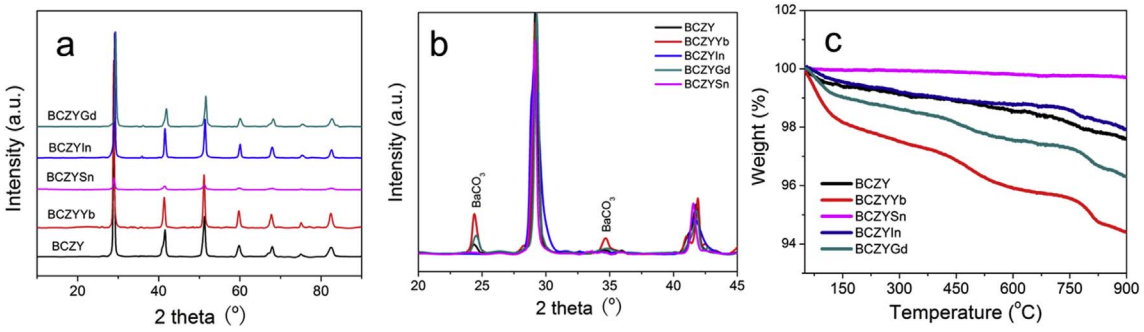

Fig. 2. XRD patterns of (a) fresh and (b) air-treated cerate samples; (c) TGA curves of air-treated cerate samples.

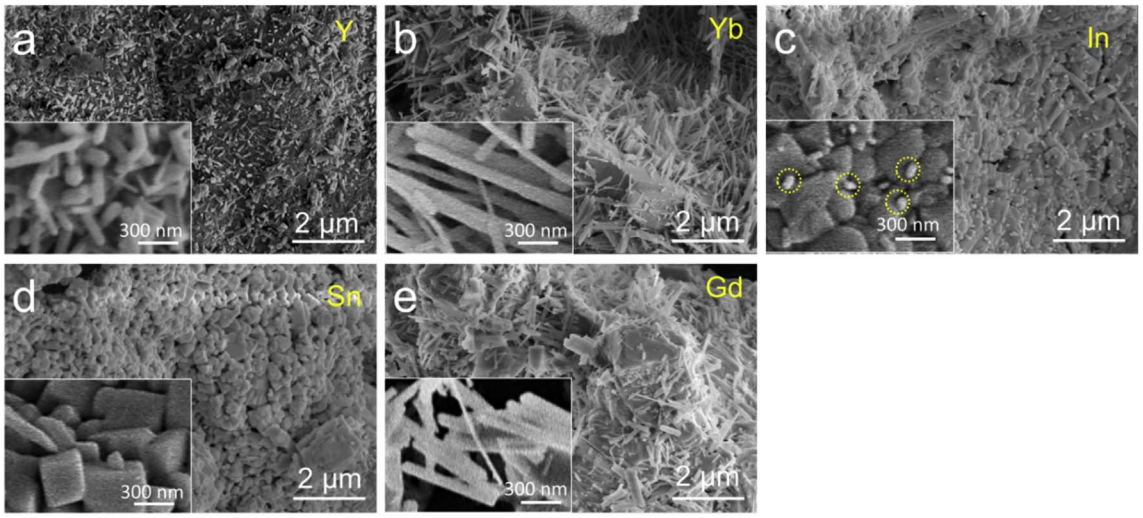

Fig. 3. SEM images of (a) BCZY, (b) BCZYYb, (c) BCZYIn, (d) BCZYSn and (e) BCZYGd after ambient-condition stability test.

Fig. 2b. The first two-step weight loss below 600 °C reflected the thermal decomposition of $MeC_xH_yO_z$ [23,24]. The last drop at ~ 800 °C correlated with the decomposition of $BaCO_3$ [25]. Interestingly, the seemingly stable BCZYIn also suffered *ca.* 2 wt% weight loss. We therefore concluded that only Sn can fully stabilize the cerate at ambient conditions. A possible reason might be that the isovalent Sn^{4+} dopant could effectively decrease the negative hydration energy of cerate, suppressing its surface hydration process. Consequently, the decomposition of cerate was unable to proceed accordingly to Eq. (1). Besides, BCZYSn also demonstrated excellent high-temperature chemical stability in humidified syngas (*vide infra*).

We then examined the morphology change of samples after the stability test. Compared to the previous observations of degraded BCZY [21], both BCZYYb and BCZYGd also showed the characteristic $BaCO_3$ nanorods on the surface (see Fig. 3), implying the superficial decomposition of the perovskite oxides (*cf.* the EDX mapping results in the ESI). Albeit that the degradation of BCZYIn was trivial, we still noticed the formation of small nanobeads, circled in the inset of Fig. 3c, on the surface. A subsequent EDX analysis confirmed that they were $BaCO_3$, corroborating the above-mentioned TGA results. To the contrary, Fig. 3d reveals that the cubic crystals of BCZYSn was sustained after the test, no newly formed phase was identified, well matching the XRD and TGA data. Hence, Sn was selected as the suitable doping element and BCZYSn was used as the candidate material of fabricating the PC-SOFC and hydrogen separation membrane.

3.3. PC-SOFCs and hydrogen separation tests

Fig. 4a shows the Arrhenius plot of the electrical conductivity of the BCZYSn disc measured in humidified hydrogen. The conductivity reached 4.2×10^{-3}, 6.8×10^{-3}, 9.7×10^{-3} and 1.1×10^{-2} S cm^{-1} at 500, 600, 700 and 800 °C, respectively, which was comparable with that of typical Sn doped cerate and zirconate [26,27]. These values were indeed lower than that of BCZYYb and BCZY, possibly because of the strong proton trapping effect in the material [28], yet BCZYSn enjoyed a balanced performance of good conductivity with much higher chemical stability at both ambient and high-temperature conditions.

We then fabricated the PC-SOFC button cell employed with the BCZYSn electrolyte. The cell was configured as the typical anode support design. Ni-BCZYSn and PBC-BCZYSn composites were respectively used as the anode and cathode in the membrane electrode assembly. The open-circuit potential (OCV) in H_2 attained 0.99 V at 600 °C (see the polarization curve in Fig. 4b), indicating the low electronic conductivity of the electrolyte material. The fuel cell was also studied when being powered by syngas. The feedstock originally comprised of certified 40% H_2 and 60% CO, simulating the major components/ratio of coal-derived syngas. However, *ca.* 5% of CO_2 was detected in the effluent of the syngas fed PC-SOFC by the gas chromatography, which was attributable to the water-gas-shift reaction at elevated temperatures. Nonetheless, the relatively high CO_2 concentration did not detriment the physico-chemical properties of BCZYSn or the performances of the cell. The maximum power densities attained 473 mW cm^{-2} and 387 mW cm^{-2} at 600 °C in humidified H_2 and syngas, respectively. The TGA data in Fig. S2 also substantiates that no carbonation reaction, which supposes to cause weight gains, occurred in 5% CO_2 balanced by N_2 (for safety reasons, TGA measurement in syngas was not conducted). The two steps of weight loss came from dehydration and the loss of non-stoichiometric oxygen. In addition, SEM image in Fig. S3 shows the unimpaired crystal morphology of BCZYSn after 24 h treatment in syngas at 600 °C.

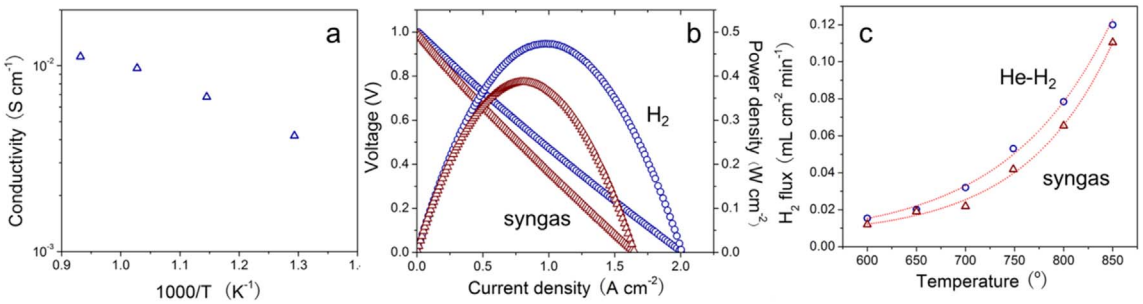

Fig. 4. (a) Arrhenius plot of the electrical conductivity of BCZYSn in humidified hydrogen; (b) polarization and power density curves of PC-SOFC in H_2 and syngas at 600 °C; (c) H_2 flux plots as a function of temperature using BCZYSn-GDC composite membrane, the feed gases were 50% H_2 + He and syngas, respectively.

Finally, we investigated the hydrogen permeability of BCZYSn. The membrane disc was consisted of 50 wt% BCZYSn and equal amount of $Gd_{0.1}Ce_{0.9}O_2$ (GDC) as the proton- and electron-conductor, respectively. When the feed gas was 50% H_2 balanced by He, the hydrogen flux reached $0.12\,mL\,cm^{-2}\,min^{-1}$ at 850 °C. This value dropped to $0.11\,mL\,cm^{-2}\,min^{-1}$ when the feedstock was switched to syngas because of the lower pH_2 according to the Wagner equation. In both scenarios, the recorded hydrogen permeability was comparable with that of various doped barium cerates [29–31]. After 24 h permeation test in syngas at 850 °C (note the presence of CO_2, see above), the H_2 flux hardly decreased, indicating the excellent stability of BCZYSn based membrane.

4. Conclusions

The present study revealed that a number of high-temperature-stable barium cerates were susceptible to the thermodynamically favored ambient-condition degradation in the presence of CO_2 and moisture. BCZYSn was, however, an exception that showed good stability in both scenarios. Along with its high protonic conductivity, it enabled excellent SOFC and hydrogen separation performances in simulated coal-derived syngas.

Acknowledgements

This work is part of the Sustainable Chemistry Research Priority Area of the University of Amsterdam (www.suschem.uva.nl). N.Y. also thanks the support from the Dutch National Science Foundation (NWO) under the project No. 729.001.022.

Appendix A. Supplementary data

Supplementary data related to this article can be found at http://dx.doi.org/10.1016/j.jpowsour.2017.12.036.

References

[1] K.D. Kreuer, Annu. Rev. Mater. Res. 33 (2003) 333–359.
[2] L. Malavasi, C.A.J. Fisher, M.S. Islam, Chem. Soc. Rev. 39 (2010) 4370–4387.
[3] R. Kannan, K. Singh, S. Gill, T. Fuerstenhaupt, V. Thangadurai, Sci. Rep. 3 (2013) 2138.
[4] S.F. Cheng, Y.J. Wang, L.B. Zhuang, J. Xue, Y.Y. Wei, A. Feldhoff, J. Caro, H.H. Wang, Angew. Chem. Int. Ed. 55 (2016) 10895–10898.
[5] E. Fabbri, L. Bi, D. Pergolesi, E. Traversa, Adv. Mater. 24 (2012) 195–208.
[6] Y.C. Zhao, C. Xia, L.J. Jia, Z.M. Wang, H.J. Li, J.S. Yu, Y.D. Li, Int. J. Hydrogen Energy 38 (2013) 16498–16517.
[7] B. Singh, S. Ghosh, S. Aich, B. Roy, J. Power Sources 339 (2017) 103–135.
[8] C.C. Duan, J.H. Tong, M. Shang, S. Nikodemski, M. Sanders, S. Ricote, A. Almansoori, R. O'Hayre, Science 349 (2015) 1321–1326.
[9] X.Z. Fu, J.L. Luo, A.R. Sanger, N. Danilovic, K.T. Chuang, Chem. Commun. 46 (2010) 2052–2054.
[10] A.B. Munoz-Garcia, M. Tuccillo, M. Pavone, J. Mater. Chem. 5 (2017) 11825–11833.
[11] B. Hua, N. Yan, M. Li, Y.Q. Zhang, Y.F. Sun, J. Li, T. Etsell, P. Sarkar, K. Chuang, J.L. Luo, Energy Environ. Sci. 9 (2016) 207–215.
[12] E. Rebollo, C. Mortalo, S. Escolastico, S. Boldrini, S. Barison, J.M. Serra, M. Fabrizio, Energy Environ. Sci. 8 (2015) 3675–3686.
[13] N.W. Ockwig, T.M. Nenoff, Chem. Rev. 107 (2007) 4078–4110.
[14] J. Hermet, M. Torrent, F. Bottin, G. Dezanneau, G. Geneste, J. Mater. Chem. 2 (2014) 9055–9066.
[15] L. Yang, S. Wang, K. Blinn, M. Liu, Z. Liu, Z. Cheng, M. Liu, Science 326 (2009) 126–129.
[16] E. Fabbri, D. Pergolesi, E. Traversa, Chem. Soc. Rev. 39 (2010) 4355–4369.
[17] F.M.M. Snijkers, A. Buekenhoudt, J. Cooymans, J.J. Luyten, Scripta Mater. 50 (2004) 655–659.
[18] M. Hakim, C.-Y. Yoo, J.H. Joo, J.H. Yu, J. Power Sources 278 (2015) 320–324.
[19] D. Konwar, N. Ngoc Thi Quynh, H.H. Yoon, Int. J. Hydrogen Energy 40 (2015) 11651–11658.
[20] L. Gui, Y. Ling, G. Li, Z. Wang, Y. Wan, R. Wang, B. He, L. Zhao, J. Power Sources 301 (2016) 369–375.
[21] N. Yan, Y.M. Zeng, B. Shalchi, W. Wang, T. Gao, G. Rothenberg, J.L. Luo, J. Electrochem. Soc. 162 (2015) F1408–F1414.
[22] N. Yan, X.Z. Fu, K.T. Chuang, J.L. Luo, J. Power Sources 254 (2014) 48–54.
[23] L.M. Dassuncao, I. Giolito, M. Ionashiro, Thermochim. Acta 137 (1989) 319–330.
[24] L.M. Dassuncao, M. Ionashiro, D.E. Rasera, I. Giolito, Thermochim. Acta 219 (1993) 225–233.
[25] I. Arvanitidis, D. Sichen, S. Seetharaman, Metall. Mater. Trans. B 27 (1996) 409–416.
[26] K. Xie, R. Yan, X. Chen, S. Wang, Y. Jiang, X. Liu, G. Meng, J. Alloy. Comp. 473 (2009) 323–329.
[27] W. Sun, M. Liu, W. Liu, Adv. Eng. Mater. 3 (2013) 1041–1050.
[28] J.A. Dawson, I. Tanaka, J. Mater. Chem. 3 (2015) 10045–10051.
[29] S. Fang, K. Brinkman, F. Chen, ACS Appl. Mater. Interfaces 6 (2014) 725–730.
[30] C. Zuo, S.E. Dorris, U. Balachandran, M. Liu, Chem. Mater. 18 (2006) 4647–4650.
[31] Y. Wei, J. Xue, W. Fang, Y. Chen, H. Wang, J. Caro, Chem. Commun. 51 (2015) 11619–11621.